The Journal of Chemical Physics

Polymer segregation in cylindrical confinement revisited: A three-dimensional free energy landscape

Cite as: J. Chem. Phys. **149**, 244906 (2018); https://doi.org/10.1063/1.5078419
Submitted: 25 October 2018 . Accepted: 05 December 2018 . Published Online: 31 December 2018

Yunfei Du, Huijun Jiang, and Zhonghuai Hou

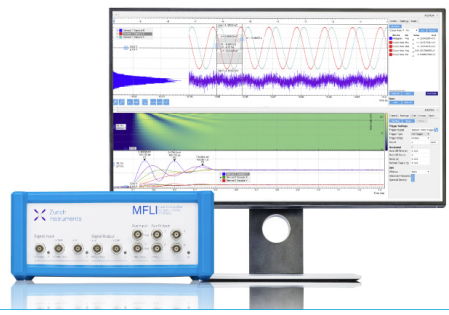

Polymer segregation in cylindrical confinement revisited: A three-dimensional free energy landscape

Yunfei Du, Huijun Jiang, and Zhonghuai Hou[a)]
Department of Chemical Physics and Hefei National Laboratory for Physical Sciences at Microscales, iChEM, University of Science and Technology of China, Hefei, Anhui 230026, China

(Received 25 October 2018; accepted 5 December 2018; published online 31 December 2018)

We study the dynamic separation process of two identical polymers confined in a cylinder, allowing both ends of the polymer chains to be free, based on a three dimensional (3D) free energy landscape combined with direct molecular dynamics (MD) simulations. The landscape suggests that the probability distribution curves of induction time (segregation time) reduced by corresponding average values would collapse into a single one under the so-called *blob constraint*, i.e., $\kappa \equiv ND^{-1/\nu}$ is a constant, where N is the number of monomers in a chain, D is the channel diameter, and $\nu \simeq 3/5$. Such a collapse behavior is well demonstrated by direct MD simulations and further by Brownian dynamics simulations of an effective particle on the 3D landscape. Interestingly, Brownian dynamics shows that the average induction time $\bar{t}_{in}$ or segregation time $\bar{t}_{se}$ decreases monotonically with κ in a power-law dependence if the diffusion coefficient $\mathcal{D}$ is fixed, suggesting a distinct mechanism of the induction process which is neither diffusion nor barrier-crossing, in accordance with trajectory analysis by using MD simulations. In addition, we find that both $\bar{t}_{in}$ and $\bar{t}_{se}$ show good power-law dependencies on the polymer length N under the *blob constraint*. *Published by AIP Publishing.*
https://doi.org/10.1063/1.5078419

I. INTRODUCTION

A polymer in geometrical confinement is not only a classical problem in polymer physics[1,2] but also related to various aspects such as single-molecule manipulations or nanofabrication in narrow pores,[3–6] viral DNA packing and injection into a host cell,[7] chromosome segregation in elongated bacterial cells,[8,9] etc. When two overlapped polymers are trapped in a cylinder, the conformational entropy is significantly reduced such that there exists an entropy force which would lead to segregation of them from each other. In the past decade, much research interest has arisen in this entropic segregation process (ESP) since it might be the essential driving force of chromosome segregation in elongated bacteria, e.g., *Escherichia coli*, while proteins implicated in the regulation of the chromosome structure and segregation may in fact function primarily in supporting such an entropy-driven segregation mechanism.[9]

In recent years, many advances have been made regarding this issue by using theoretical analysis combined with molecular dynamics (MD) simulations. A variety of different aspects influencing the ESP have been considered, ranging from polymer stiffness,[10–12] crowding effects,[13–16] and topological structures of the polymer chain (linear, ring, or star).[17–19] Of particular interest, it is found that there exists an induction process where the initial symmetry of the system has to be broken before the ESP can set in, which may extremely delay the separation process. Indeed, recently experiments revealed that a process called sister chromatid cohesion, i.e., the period between the time a locus is replicated and the visual separation of the two sister loci, widely exists in living cells. Such an induction behavior is essential for genome stability since it is required for both high fidelity chromosome segregation and DNA damage repair.[20–22] In an early paper, Arnold and Jun argued that the induction behavior is due to the thermal diffusion of the polymer.[18] Under this assumption, they concluded that the average induction time $\bar{t}_{in}$ is proportional to N^3 with N being the polymer length (the number of monomers), which is much larger (slower) than the N^2 scaling of the average segregation time $\bar{t}_{se}$. In a subsequent study, however, Minina and Arnold argued that the induction is a rare event and the main mechanism is not the diffusion of the whole chain but rather the arrangement of chain ends. Using the de Gennes blob model which represents the polymer as a chain of blobs, they obtained a free energy landscape as a function of the number of overhanging blobs, which allows them to estimate the induction time by using Kramer's rate theory, showing an exponential dependency on the number of monomers.[23,24] The authors also used MD simulations to test the theoretical predictions, showing qualitative agreements with the theory despite some quantitative discrepancies.

Note that, however, Minina and Arnold had considered a simplified case where they allowed the chains to partially segregate only at one end of the chains in both theory and simulations, by fixing the rightmost beads to prevent diffusion. Such a simplified model is justified if the chains are sufficiently long because two sides of polymers would then

a)Author to whom correspondence should be addressed: hzhlj@ustc.edu.cn

hardly influence each other.[23] In some real systems, however, this infinite-long chain approximation may not be applicable. For instance, the typical parameters of *E. coli* measured experimentally are $D \approx 5$ for the channel diameter, $L \approx 28$ for the channel length, and $N \approx 200$ for the polymer length, scaled by the size of a structural unit (70 ± 20 nm).[25] Therefore, the segregation process should be considered with both ends being free for these finite chains. Nevertheless, such a more realistic model has not been systematically studied yet, to the best of our knowledge.

Motivated by this, in the present paper, we have studied the segregation behavior of two self-avoiding polymers each with N beads in an infinitely long cylinder with diameter D, by using both theory and MD simulations. As stated above, we allow that both two ends of the polymer chains are free of extra constraints. Applying the renormalized Flory theory, we get a three dimensional (3D) free energy landscape as a function of two free parameters, namely, the fraction of overhanging monomers of one chain over the other on the left side, x, and that on the right side y. The 3D landscape clearly shows two valley regions in the first and third quadrants, corresponding to two temporarily trapped states with one chain inside another. Starting from the initial condition with $x = y = 0$, the system may get trapped into these valley regions for a while, corresponding to the induction process, after which the two chains become separated. The landscape $U(x, y)$ is the same if one introduces the so-called *blob constraint*, i.e., setting $\kappa \equiv ND^{-5/3} = \text{const}$. Such a feature indicates that the probability distribution function (PDF) of the induction time t_{in} and the segregation time t_{se} would both collapse into a single curve, if rescaled by the corresponding averaged values $\bar{t}_{in}$ and $\bar{t}_{se}$, respectively, which is confirmed by MD simulations. Furthermore, we have taken a Brownian dynamics (BD) simulation of an effective particle on the landscape $U(x, y)$ with diffusion coefficient $\mathcal{D}$, and the PDFs for $t_{in}/\bar{t}_{in}$ ($t_{se}/\bar{t}_{se}$) can match very well with those obtained from MD simulations, further demonstrating the validity of the free energy description. Interestingly, the BD simulation results show that both $\bar{t}_{in}$ and $\bar{t}_{se}$ show very good power-law decreasing dependencies with κ if the diffusion coefficient $\mathcal{D}$ is fixed, suggesting a distinct mechanism of the induction process which is neither diffusion nor barrier-crossing. By analyzing the trajectories from MD simulations, we have found that after the system falls into the trapped valley region with $xy > 0$, it actually meanders randomly around the local minima until it finally enters into a released region with $xy < 0$. Finally, we have studied the relationships between $\bar{t}_{in}$ ($\bar{t}_{se}$) and N. Surprisingly, $\bar{t}_{in}$ ($\bar{t}_{se}$) presents a well scaling relationship with N if the *blob constraint* is introduced ($\kappa = \text{const}$), which may be closely related to the effective diffusion coefficient $\mathcal{D}$ on the 3D landscape. Gathering all these results above, we suggest a scaling ansatz for the induction (segregation) time as $\bar{t}_{in(se)} \sim N^{\alpha(\kappa)}\kappa^{c}$, where the scaling exponents $\alpha(\kappa) > 0$ and $c < 0$ are different for induction and segregation.

The paper is organized as follows. In Sec. II, we describe the simulation method. In Sec. III, we present the theoretical method and draw the free energy landscape. Simulation results and discussion are presented in Secs. IV and V followed by conclusion in Sec. VI.

II. SIMULATION METHOD

We consider two identical polymers confined in a cylinder with diameter D. The cylinder is infinitely long at both two ends, and each polymer is represented as a bead-spring chain of N beads with diameter σ, linked by spring-like bonds. The bead-bead and bead-wall interactions are modeled by the fully repulsive Weeks-Chandler-Andersen (WCA) potential[26]

$$U_{WCA}(r) = \begin{cases} 4\epsilon\left[(\frac{\sigma}{r})^{12} - (\frac{\sigma}{r})^{6} + \frac{1}{4}\right], & r < 2^{\frac{1}{6}}\sigma \\ 0, & r \geq 2^{\frac{1}{6}}\sigma \end{cases}, \quad (1)$$

where ϵ represent the potential strength and r denotes the distance between two bead centers or the bead center and the wall. The bond interaction between two nearby beads in the chain is described by the FENE (finite extensible nonlinear elastic) potential[27]

$$U_F(r) = -\frac{1}{2}\epsilon_F r_F^2 \ln\left[1 - (\frac{r}{r_F})^2\right], \quad (2)$$

where ϵ_F is the interaction strength and r_F is the maximum stretch of r. The dynamics of the polymer beads are described by the following Langevin equations:

$$m\frac{\mathrm{d}^2\mathbf{r}}{\mathrm{d}t^2} = -\gamma\frac{\mathrm{d}\mathbf{r}}{\mathrm{d}t} - \nabla_{\mathbf{r}}U + \sqrt{2k_BT\gamma}\boldsymbol{\xi}(t), \quad (3)$$

where $U = \sum U_{WCA}(r) + U_{FENE}(r)$, $\mathbf{r}$ is the position vector, m is the bead mass, T is the temperature, γ is the friction coefficient of the bead in the background solvent, and $\boldsymbol{\xi}(t)$ denotes independent Gaussian white noises with zero means and unit variances, i.e., $\langle\boldsymbol{\xi}(t)\rangle = 0$, $\langle\boldsymbol{\xi}(t)\boldsymbol{\xi}(t')\rangle = \mathbf{I}\delta(t - t')$, where $\mathbf{I}$ is the unit tensor. We nondimensionalize the equations of motion above using σ and k_BT as basic units of length and energy, respectively, and m as the unit of mass. A time unit is rescaled by $\tau = \sigma\sqrt{m/(k_BT)}$. The dimensionless friction coefficient γ is set to 1.0, and parameters for the WCA potential are $\epsilon = k_BT$ and for the FENE potential are $\epsilon_F = 10k_BT$ and $r_F = 2.0\sigma$. This system is simulated by using the simulation package Espresso 3.3.1.[28] The velocity-Verlet algorithm is used to simulate the dynamic equation with a time step $\Delta t = 0.01\tau$. The initial configuration is a *ladder*, wherein the ith bead of one chain is connected to the ith bead of the other chain.[18,23,24] Perhaps a less artificial way could be that two parallel linear chains are linked in the middle by a temporary bond,[11] but this alternative way nearly makes no quantitative difference to the final results. After sufficient steps of simulations to warm the system, we remove the interconnecting bonds between the chains and start to study the segregation process.

III. THEORY

The dynamics of the system begins with the initial (I) state, as shown in Fig. 1(a). Upon fluctuation, the two polymers may change the state via switching the ends. As shown in Fig. 1(b), both ends of polymer 1 may overhang those of polymer 2, with N_x (N_y) monomers at the left (right) side, respectively. To avoid ambiguity, we define $N_x > 0$ ($N_y > 0$), if the end of polymer 1 overhangs the end of polymer 2 in the same side. For the state shown in Fig. 1(b), both $N_x > 0$ and $N_y > 0$ such

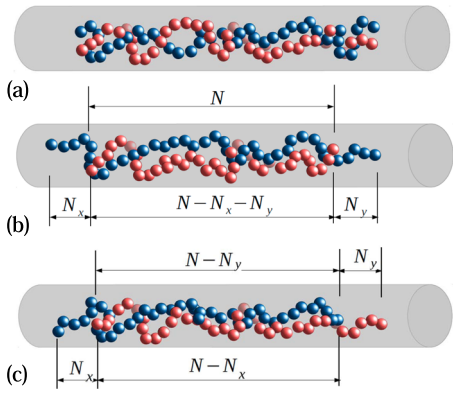

FIG. 1. (a) Initial state. Both ends at left (right) side of two polymers are at the same position. (b) Trapped state. The red chain labeled polymer 2 is trapped by the blue chain labeled polymer 1 totally, and the segregation is forbidden. The overhangs along two side of polymer 1 are $|N_x|$ and $|N_y|$. Part in the overlap region is N for polymer 2 and $N - |N_x| - |N_y|$ for polymer 1. (c) Released state. Both of two chains have a part overlapped but not all. For polymer 1, $|N_x|$ monomers overhanged and $N - |N_x|$ overlapped. While for polymer 2, $|N_y|$ overhanged and $N - |N_y|$ overlapped.

that polymer 2 is totally nested in polymer 1, corresponding to a trapped (T) state. In the middle overlapped region, the number of monomers is $N - |N_x| - |N_y|$ for polymer 1 and N for polymer 2. Note that $N_x < 0$ and $N_y < 0$ correspond to another trapped state with polymer 1 all nested in polymer 2. For the state shown in Fig. 1(c), we have $N_x > 0$, $N_y < 0$ and the two chains would start to segregate, corresponding to a released (R) state.

Using the renormalized Flory theory,[29] we can calculate the free energy of the system as a function of the two free parameters N_x and N_y. A polymer with N monomers confined in a cylinder with diameter D can be equivalent to a sequence of blobs arranged closely[2] wherein one blob consists of $g \sim D^{1/\upsilon}$ ($\upsilon \simeq 3/5$ in three dimensions) monomers. The chain thus has $n_b = N/g \sim ND^{-5/3}$ blobs, and the total free energy of the chain is given by $U = n_b f_b \sim ND^{-5/3} f_b$, where f_b denotes the free energy for a blob which is a non-universal constant depending on the type of polymer. And the extended length of the chain is given by $L = n_b D \sim ND^{-2/3}$. For two polymers confined in the cylinder, basically, the overlapped parts can be treated as two single polymers trapped in effective sub-cylinders of diameters $D_1 = D\sqrt{\alpha}$ and $D_2 = D\sqrt{1-\alpha}$,[23,24,30] respectively, where α denotes a partition coefficient. For the initial I-state, we have $\alpha = 1/2$ and $D_1 = D_2 = D/\sqrt{2}$, thus the total free energy reads $U_I \sim 2N\left(D/\sqrt{2}\right)^{-5/3} f_b$. In the following, for simplicity, we will just set $f_b = 1$ and write $U_I = 2^{11/6} ND^{-5/3}$. For the T- or R-states, one can obtain the partition coefficient α using the condition that the extended lengths of both polymers are the same in the overlapped region. Then we can calculate the free energy of each polymer in the overlapped or overhanging region, summing up them to get the total free energy. For more details, please see the Appendix.

Consequently, the total free energy U of the system is given by

$$U = \begin{cases} U_T(x,y) & \text{for } xy \geq 0 \\ U_R(x,y) & \text{for } xy \leq 0, \end{cases} \tag{4}$$

where $x = N_x/N$ and $y = N_y/N$ are two dimensionless parameters, $U_T(x,y)$ is the free energy for the T-state ($xy \geq 0$) given by

$$U_T(x,y) = ND^{-5/3}\Big\{\Big[1 + (1-|x|-|y|)^3\Big]^{5/6} \times \Big[1 + (1-|x|-|y|)^{-3/2}\Big] + |x| + |y|\Big\} \tag{5}$$

and $U_R(x,y)$ is the free energy of the R-state ($xy \leq 0$) given by

$$U_R(x,y) = ND^{-5/3}\Big\{\Big[(1-|x|)^3 + (1-|y|)^3\Big]^{5/6} \times \Big[(1-|x|)^{-3/2} + (1-|y|)^{-3/2}\Big] + |x| + |y|\Big\}. \tag{6}$$

For $x = y = 0$, $U_T = U_R = 2^{11/6} ND^{-5/3}$ which coincides exactly with the free energy of the initial state U_I.

IV. RESULTS

A. 3D free energy landscape

Equations (4)–(6) constitute the main theoretical results of the present work. In Fig. 2, a 3D plot of the free energy landscape $U(x,y)$ is presented. The landscape shows two apparent valleys in the 1st and 3rd quadrants, where $xy > 0$. According to Eq. (5), the free energy $U_T(x,y)$ is constant along the lines $x + y = \text{const}$; hence, the valleys are flat along the direction given by these lines. And the motion along these

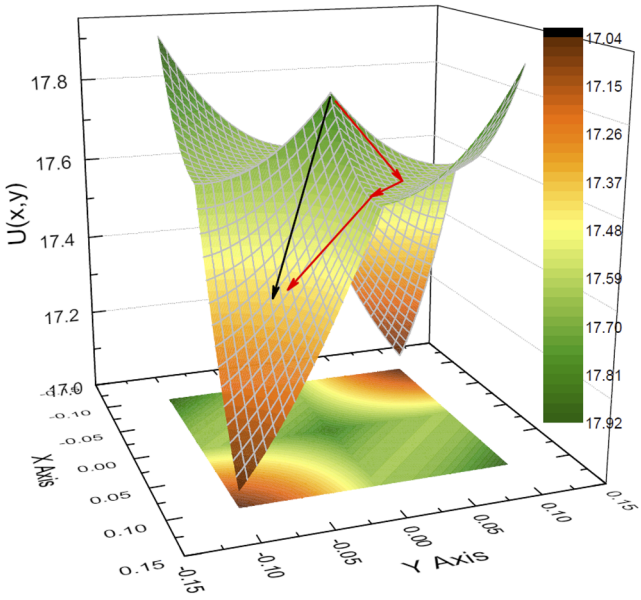

FIG. 2. Confined free energy landscape in three dimensions with a projection on the bottom and a color bar attached. The unit of $U(x, y)$ is f_b, where f_b denotes the free energy for a blob, and the key parameters to generate such a landscape are $D = 6$, $N = 100$. The middle point ($x = 0$, $y = 0$) represents the initial state. And the green region and the yellow region represent the trapped (T) state and the released (R) state, respectively. To get a distinct illustration, only the ranges of x and y in $-0.1 \sim 0.1$ are showed. It is clear that the landscape in the R-state is sharply decreasing and the landscape in the T-state shows two apparent valleys. And the black arrow and the red arrow represent two choices of traces from the initial state. If the system moves in the direction of the black arrow, this will lead to a segregation process. However, if the system falls into the T-state accidentally, in the direction of the red arrow, this will lead to an induction process until it finally enters into the R region.

directions can be viewed as that the nested polymer moves relative to the outer polymer in a diffusive manner such that the total overhang of the outer polymer stays constant, while the length of one overhang decreases and the other increases. Therefore, there exist two metastable T-states, one in the 1st and the other in the 3rd quadrant. By contrast, the landscape in the 2nd or 4th quadrant is monotonically decreasing with a sharp slope upon increasing distance from the initial state $x = y = 0$, indicating that the R-state is a spontaneous process.

The landscape shown in Fig. 2 clearly illustrates the overall picture of the segregation process. Clearly, the initial state is unstable since it locates at a local maximum on the landscape. The configuration of the two polymers will change, either to the T-states with $xy > 0$ or R-states with $xy < 0$. If the system changes to R-states, as indicated by the black arrow in Fig. 2, the segregation process will immediately take place and no induction behavior exists. However, if by chance the system changes to the T-states, as shown by the red line in the figure, it may get trapped in the valley region for a while before it reaches the edge and then get released. In this latter case, there will be an induction process before the segregation would take place.

In Fig. 3(a), we have chosen two typical trajectories of the system obtained from direct simulations and projected them onto a x-y parameter plane. The black trajectory mainly stays in the 4th quadrant corresponding to a direct separation process without induction time. The distance R_{c2c} between centers of mass of the two chains increases sharply from the very beginning, as shown in Fig. 3(b). By contrast, the red trajectory first goes to the valley area in the 3rd quadrant, where it performs random walk for a period of time, before it finally drops into the 2nd quadrant and gets separated. Accordingly, the distance R_{c2c} remains very small for a quite long period of time before it grows monotonically, as also shown in Fig. 3(b). This trajectory clearly demonstrates the induction process with an induction time to be about 300 in dimensionless time unit. However, to quantitatively get the induction time t_{in} as well as the segregation time t_{se}, a clear definition on them is necessary and we achieve this by the following procedure. First, we need to define several states to depict the configuration of polymers. If the beads from two polymers do not overlap along the cylinder, such configuration is labeled "D" state which means that these two polymers are totally dismissed or separated from each other. Else if one polymer is totally covered by another polymer at two ends, the system is in induction and such configuration is labeled "I" state, otherwise "S" state which corresponds to a segregation state. So for a whole process, one can get a time sequence labeled, for example, "I I . . .ISISI I I SSSS. . .DSDDDD. . .." Then, one can search the time sequence from back to front until first we find the "D" state and "S" state and define these two time intervals from very beginning as t_{tot} and t_{in}, respectively, surely, $t_{tot} = t_{in} + t_{se}$. Finally, both t_{in} and t_{se} are exactly obtained.

B. Distributions of induction and segregation time

The 3D free energy landscape allows us to investigate the segregation process as the diffusion motion of an effective particle, which can be described by the following Fokker-Planck equation (FPE):

$$\frac{\partial P(\mathbf{r},t)}{\partial t} = \mathcal{D}\nabla e^{-\beta U(\mathbf{r})}\nabla e^{\beta U(\mathbf{r})}P(\mathbf{r},t), \tag{7}$$

where $\mathbf{r} = (x, y)$ and $\mathcal{D}$ denotes the effective diffusion coefficient on the free energy space. We note here that this $\mathcal{D}$ should generally depend on the chain length N and the channel width D and even may depend on the position $\mathbf{r}$. For simplicity here and as an assumption, we set $\mathcal{D}$ to be a constant independent of $\mathbf{r}$. If one rescales time by $t' = \mathcal{D}^{-1}t$, then one has $\partial P/\partial t' = \nabla\, e^{-\beta U}\nabla e^{\beta U}P$ and then the probability distribution function $P(\mathbf{r}, t')$ would be determined by the free energy landscape $U(\mathbf{r})$ only. We also note that there is an important feature shown in Eqs. (5) and (6), i.e., $U(x, y) \equiv ND^{-5/3}u(x, y)$, where $u(x, y)$ is a function of the dimensionless variables x, y and not dependent on the parameters N and D. Therefore, if the parameter $\kappa = ND^{-5/3}$ is fixed to be a constant, as called *blob constraint* in the rest of paper, then $P(\mathbf{r}, t')$ would be the same after rescaling the time by $\mathcal{D}^{-1}$. Since the probability distribution function determines all the statistical properties of the system,

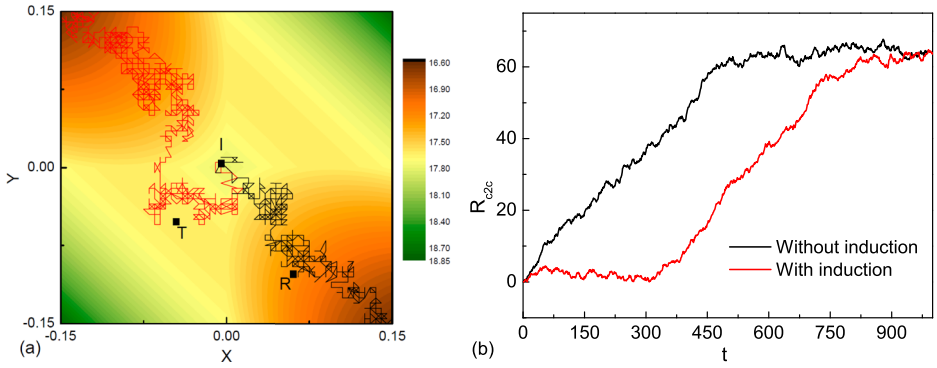

FIG. 3. (a) The real traces from direct simulations in the projection of the free energy landscape. The red one corresponds to a typical process with induction, and the black one corresponds to a directed segregation process. As we count the number of monomers overhanged along two side and rescale it to x or y by N, the trace is connected by a list of discrete points. The black square dots labeled "I," "T," and "R" represent the initial point, trapped region, and released region, respectively. (b) The time dependency of the distance between two centers of mass of the polymer. The red and black curves correspond to the processes with and without an apparent induction, respectively. These two curves are chosen as the typical examples to highlight the induction time. An example simulation runs for $D = 4$, $N = 100$ with a sampling for every 100 time steps.

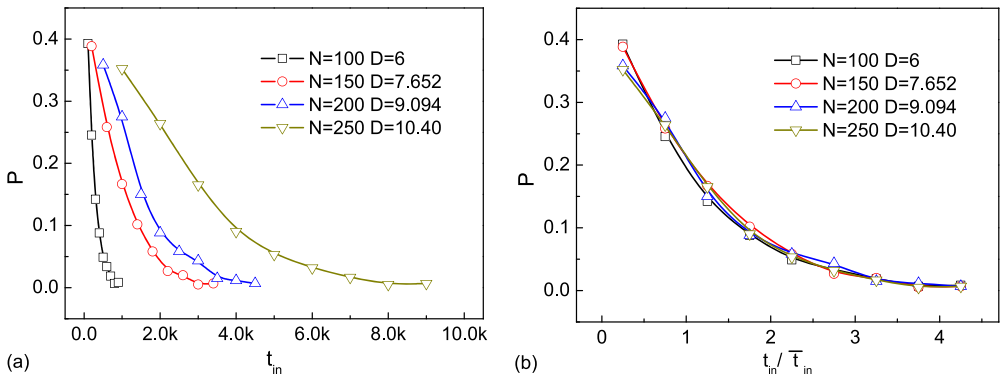

FIG. 4. Probability distribution functions of induction time no-rescaled (a) and rescaled (b) by the average value. Each setting of N and D in the curve is under the constraint of $N/D^{5/3} = \kappa = 5.047$ by using the setting of $N = 100$, $D = 6$ as the base. The lines with different colors are drawn to guide the eyes.

one would then expect that the distribution of the induction (segregation) time $t_{in}(t_{se})$ as well as its average value $\bar{t}_{in}(\bar{t}_{se})$ would be the same under these constraints (fixed κ and rescaled by $\mathcal{D}^{-1}$).

To validate this point, we have performed direct MD simulations to obtain the distributions of the induction time t_{in} for a few different parameter sets of N and D. Figure 4 shows the probability distribution function (PDF) for t_{in} for fixed $\kappa = 5.047$ but different values of N and D. In Fig. 4(a), the PDFs are depicted without rescaling the time. Obviously, the PDFs for different N and D do not collapse, although the shapes are quite similar. As stated in the last paragraph, one would expect that the distribution should be the same if the time is rescaled by $\mathcal{D}^{-1}$. Unfortunately, here we do not know the exact value of $\mathcal{D}$ as well as its dependence on N and D. Note that, however, the average induction time $\bar{t}_{in}$ should be proportional to $\mathcal{D}^{-1}$, given that $U(\mathbf{r})$ is the same according to Eq. (7). Therefore, one may rescale the induction time by its average value $\bar{t}_{in}$, and the rescaled distribution should collapse if the landscape really works. This is indeed the case, as shown in Fig. 4(b), where the PDFs are shown with the time rescaled by the average values $\bar{t}_{in}$ and all the curves now almost collapse into a single line. Such a collapse indicates that the free energy landscape does work well to describe the dynamics of the system.

For the segregation process, which corresponds to a motion along the downhill in the 2nd or 4th quadrant to the R-state, the average time can be obtained via calculating the time for the effective particle to reach some boundaries. As shown in Fig. 3(b), the two polymers can be viewed as separated if the distance of their centers-of-mass surpasses some threshold value d_c. For a rough estimation, one can just assume that the effective particle performs an overdamped motion along the direction $x = -y$ subjected to a drift force $f_{dr} = -\nabla_{x=-y}U(x, y)$ and an effective friction $\gamma = (\beta\mathcal{D})^{-1}$. The average velocity of the particle thus reads $\bar{v} \simeq \bar{f}_{dr}/\gamma = \beta\mathcal{D}\bar{f}_{dr}$, where $\bar{f}_{dr}$ is the average drift force along the downhill direction $x = -y$, which depends on the details of $U(x, y) = \kappa u(x, y)$ and is also proportional to the parameter κ. The average time $\bar{t}_{se}$ can then be approximately given by $\bar{t}_{se} \sim d_c/\bar{v} \propto (\kappa\mathcal{D})^{-1}$. Such a simple analysis shows that the average segregation time also scales as $\mathcal{D}^{-1}$, the same as the case for the induction time. Therefore, the distribution function for the segregation time t_{se} should also be the same after rescaling with the average value $\bar{t}_{se}$.

In Fig. 5, we show the PDFs for t_{se} obtained from simulations for fixed $\kappa = 5.047$. Different from that of induction time t_{in}, the PDF for t_{se} looks like a Gaussian distribution with an apparent single peak around the average value $\bar{t}_{se}$. The distribution shows a little bit long tail, which is probably due to the random motion perpendicular to the direction that landscape decreases. In Fig. 5(a), the PDFs are drawn without rescaling time, while in (b) they are drawn with rescaling with the

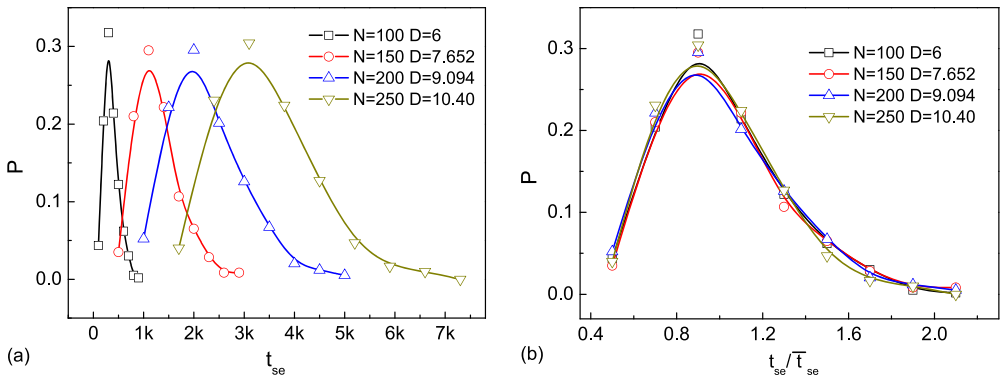

FIG. 5. Probability distribution functions of segregation time no-rescaled (a) and rescaled (b) by the average value, respectively. Each setting of N and D in the curve is under the constraint of $N/D^{5/3} = constant$ by using the setting of $N = 100$, $D = 6$ as the base. The lines with different colors are drawn to guide the eyes.

average segregation time $\bar{t}_{se}$. Again the curves collapse rather well in good agreements with the theoretical predictions made above based on the 3D free energy landscape.

C. Brownian simulation with $\mathcal{D} = 1$

The above analysis demonstrates that the 3D free energy $U(x, y)$ can indeed qualitatively describe the dynamic behavior of polymers in a confined channel. The rescaled PDFs of t_{in} and t_{se} shown in Figs. 4(b) and 5(b) actually reflect the features of $U(x, y) = \kappa u(x, y)$. To further check the validity of this free energy function, one may compare directly these rescaled PDFs obtained from MD simulations with those predicted by the FPE [Eq. (7)]. However, the analytical results of these PDFs are not available for this complicated free energy landscape.

To proceed, we note that the FPE corresponds to an overdamped Langevin equation as follows:

$$\dot{\mathbf{r}} = -\beta\mathcal{D}\nabla U(\mathbf{r}) + \sqrt{2\mathcal{D}}\boldsymbol{\zeta}(t), \tag{8}$$

where $\boldsymbol{\zeta}(t)$ denotes a Gaussian white noise with zero mean and $\langle\boldsymbol{\zeta}(t)\boldsymbol{\zeta}(t')\rangle = \delta(t - t')\mathbf{I}$ with $\mathbf{I}$ being the unit tensor. One can then perform Brownian simulations of Eq. (8) to obtain the distributions of the induction and segregation times. Note that, by doing so here, the whole system is equivalent to an effective particle on the landscape $U(x, y)$. Surely the simulation of this overdamped Langevin equation is much cheaper than the original MD simulation. Since we only need to obtain the rescaled PDF, the value of $\mathcal{D}$ would not affect the final results. Therefore, we can set $\mathcal{D} = 1$ for simplicity and let κ be the only free parameter.

In Fig. 6(a), the PDFs of the rescaled induction time $t_{in}/\bar{t}_{in}$ obtained from Brownian simulations (solid line) and direct MD simulations (dashed line) are shown for two different values ofκ, respectively. Physically, a larger κ indicates a stronger constraint in the channel and a deeper potential valley for the T-state. Interestingly, both distributions of $\kappa = 3.125$ and $\kappa = 19.84$ show a typical feature of multiple time scales (note that the left axis is in logarithmic scale), i.e., the curve is not a straight line but composed of two segments with different slopes. The PDFs of the rescaled segregation time $t_{se}/\bar{t}_{se}$ are shown in Fig. 6(b). Different from the distribution of the induction time, the PDF for t_{se} has a clear cut peak around the average value $\bar{t}_{se}$. If κ is large, e.g., $\kappa = 19.84$, the slope of the landscape is relatively sharp and the distribution is typically Gaussian concentrated around $t_{se}/\bar{t}_{se} = 1.0$. For a small $\kappa = 3.125$, one can see that the distribution is wider and the peak shifts to a smaller value with $t_{se}/\bar{t}_{se} < 1$, probably due to the fact that the landscape is relatively flat and the system would perform more random motion perpendicular to the decreasing direction of the landscape. Note that for both t_{in} and t_{se}, the rescaled distributions obtained from Brownian simulations agree rather well with those obtained from direct MD simulations, further demonstrating the validity of the free energy landscape.

Using Brownian simulations, we can obtain the induction time $\bar{t}_{in}$ and $\bar{t}_{se}$ as a function of κ given $\mathcal{D} = 1$. The results are shown in Fig. 6(c). Both $\bar{t}_{in}$ and $\bar{t}_{se}$ decrease monotonically with κ since a larger κ corresponds to a sharper slope to release. Very interestingly, we find both $\bar{t}_{in}^{\mathcal{D}=1}$ and $\bar{t}_{se}^{\mathcal{D}=1}$ show very good power-law scaling with κ. Overall, $\bar{t}_{se}^{\mathcal{D}=1}$ is larger than $\bar{t}_{in}^{\mathcal{D}=1}$, while the scaling exponent for $\bar{t}_{in}^{\mathcal{D}=1}$ is larger (decaying faster) than that of $\bar{t}_{se}^{\mathcal{D}=1}$. Nevertheless, why both $\bar{t}_{in}$ and $\bar{t}_{se}$ show such good power-law dependencies with κ is quite interesting and still open to us.

D. Mechanism of induction behavior

The power-law decay of $\bar{t}_{in}^{\mathcal{D}=1}$ with κ is quite nontrivial. In Ref. 23, it was suggested that the induction process is a rare-event barrier-crossing process such that the induction time shows an exponential dependency on $\kappa = ND^{-5/3}$, i.e., $t_{in} \sim D^2N\exp\left(cND^{-5/3}\right)$, but being exponentially increasing rather than decreasing. Therein, a larger κ corresponds to a deeper free energy minimum such that it is harder for the system to escape the metastable T-state, leading to a longer induction time. Here, however, the induction behavior is due to the stay of the system in the valley area and it ends with the system changing into the R-state, so the barrier-crossing process is not energetic favorable and the use of Kramer's theory maybe not justified. And a larger κ would lead to a sharper slope down the initial point, which would lead to a smaller induction

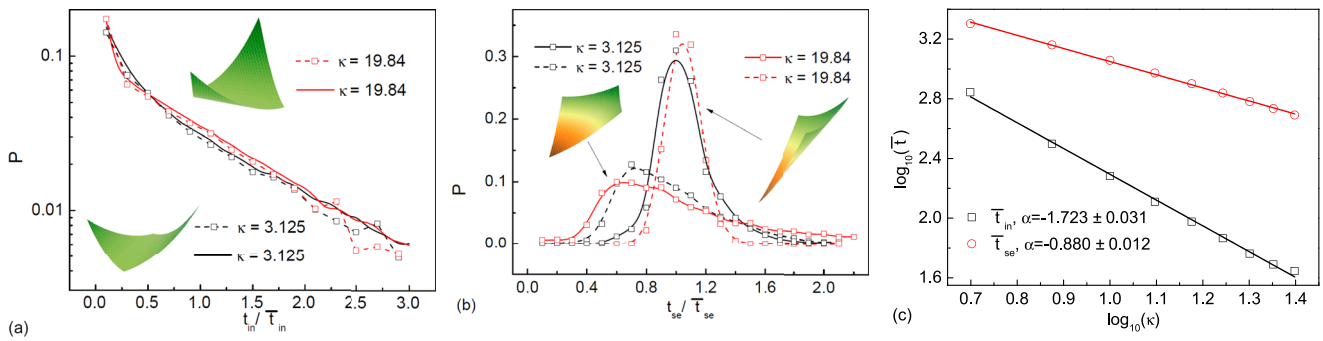

FIG. 6. Probability distribution functions of the induction time (a) and segregation time (b) rescaled by the average value. In both (a) and (b), the solid lines correspond to the results from Brownian simulations, while the dashed lines correspond to the results from direct MD simulations. Besides two different values of κ, 3.125 and 19.84, are studied and labeled in red and black, respectively. In direct MD simulations, $\kappa = 3.125$ and $\kappa = 19.84$ are achieved approximately by setting ($N = 100$, $D = 8.0$) and ($N = 200$, $D = 4.0$), respectively. (c) Average induction time $\bar{t}_{in}$ and $\bar{t}_{se}$ as a function of κ given $\mathcal{D} = 1$, obtained from Brownian simulation results.

time. Therefore, the mechanism of the induction behavior in our present study is quite different from the previous ones. For a similar reason, a larger κ would also lead to a faster segregation process once the system enters into the R-state region.

To further demonstrate this point, we cut out the induction part of the trajectories from real MD simulations and project it to the x-y plane. To do so, we have got the density distribution or probability distribution of finding the system on the x-y plane. The contour plot of this distribution is depicted in Figs. 7(a) and 7(b) for $N = 400$, $D = 9.153$ and $N = 400$, $D = 6.063$, corresponding to $\kappa = 9.921$ and $\kappa = 19.84$, respectively. Clearly, the induction trajectories mainly stay in the deepest valley region around the energy minima of the free energy landscape, as plotted in Fig. 2. Once the trajectory goes across the boundary at the x axis or y axis, it will go down the slope such that the segregation takes place. Very interestingly, both Figs. 7(a) and 7(b) show that the induction traces can also enter into the R-state region, which means that the system would visit the R-state region for a while and return back to the T-state region before it formally begins a segregated process. However, the density condensed regimes in 1st and 3rd quadrant cannot quantitatively map the energy minima of theoretical prediction. This probably due to the finite-size effect that the number of beads in a blob in the present work may not be enough to support a de Gennes scaling, and the exact scaling exponent $\upsilon \simeq 3/5$ may need a correction.

Note that the trajectory can cross the boundaries between T-state and R-state at any point on the axis, before or after it reaches the bottom of the valley. Therefore, it would be helpful to investigate how these crossing points distributed along the axis, which would give more insight about the induction process. In Fig. 7(c), the probability distribution of the crossing points as a function of the distance from the initial point is depicted, e.g., for $\kappa = 9.921$ and 19.84, in accordance with Figs. 7(a) and 7(b), respectively. For a relatively small $\kappa = 9.921$, the distribution is more flat than that for a larger $\kappa = 19.84$. Note that the line for the valley bottom in 1st and 3rd quadrants reads $x + y \simeq 0.065$, which intersects the axis at two points with distance 0.065 to the initial point. For these two values of κ, the crossing points mainly concentrate around 0–0.1 and decrease monotonically with distance from the initial point. This is confusing at first glance. Due to the fact that the energy minima in the induction regime are at $x + y \simeq 0.065$, and the distribution of the cross point seems to look like non-monotonic and concentrated around 0.065. However, as shown in Figs. 7(a) and 7(b), the extension is wider along the direction $x + y = const$ as the system is approaching the energy minima, and then it would take more time to reach the boundaries between T-state and R-state. Meanwhile, such a monotonic decreasing property also indicates that most of the induction trajectories actually enter into the R-state region rapidly instead of entering into the valley bottom. If in case the system drops into such valley bottom, it would take much long time to meander around this region, as shown in the darker region in Figs. 7(a) and 7(b), which results in a long tail in Fig. 7(c). So farther away from the initial point, the probability of finding the system still in the T-state is smaller and the corresponding induction time is longer. This is greatly in accordance with the decreasing dependency of PDFs with t_{in} in Fig. 4. However, for a smaller $\kappa = 9.921$, the valley is shallow such that there is more chance for the trajectory to stay at the slope and more probably visit the R-state region for a while, and then the density distribution is wider, as shown already in Fig. 7(b). Such a scenario for induction is clearly distinct from a barrier-crossing picture.

E. Dependencies of $\bar{t}_{in}$ and $\bar{t}_{se}$ on N for fixed κ

In previous studies on the segregation process but with one end fixed,[23] the authors assumed that the diffusion coefficient $\mathcal{D}$ is dominated by the outermost blob and therefore scales as $1/g \sim D^{-5/3}$. However, in a more realistic segregation process with both ends free, and the diffusion coefficient $\mathcal{D}$ is not simply determined by the end blob but may depend on the whole polymer chain. Unfortunately, the dependence of $\mathcal{D}$ on N or D is not available at the current stage.

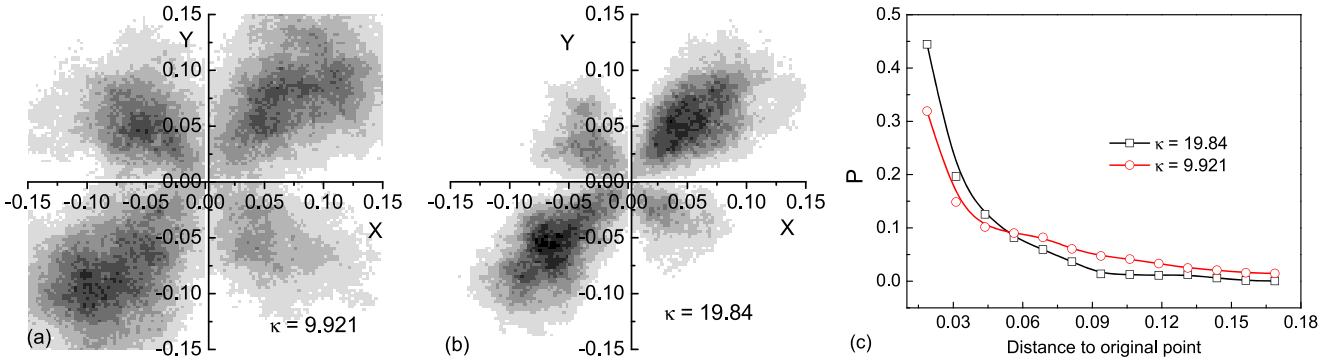

FIG. 7. (a) and (b) Density distribution function of the induction trajectories in the phase space (x, y), where (a) and (b) correspond to the system with $\kappa = 9.921$ ($N = 400$, $D = 6.063$) and $\kappa = 19.84$ ($N = 400$, $D = 9.153$), respectively. For both (a) and (b), the range of density distribution in 1st and 3rd quadrants is larger than that in 2nd and 4th quadrants and, apparently, there are two density accumulated areas in 1st and 3rd quadrants, which correspond to the local energy minima. (c) Probability distribution of the crossing points as a function of the distance from the initial point. The black square represents a $\kappa = 19.84$ case, while the red square represents a $\kappa = 9.921$ case. For the two values of κ, the crossing points mainly concentrate around this distance about 0–0.1 and decrease with distance from the initial point, while the probability distribution for $\kappa = 19.84$ looks steeper than the case for $\kappa = 9.921$. The solid lines are drawn to guide the eyes.

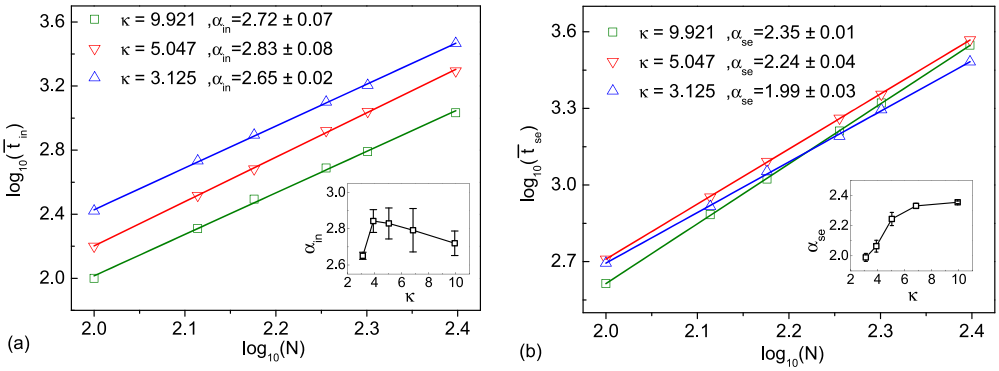

FIG. 8. The scaling relation of $\bar{t}_{in}$ (a) and $\bar{t}_{se}$ (b) with N under the constraint $N/D^{5/3} = \kappa$ by using the value of 9.921, 5.047, and 3.125, which correspond to using ($N = 100$, $D = 4.0$), ($N = 100$, $D = 6.0$), and ($N = 100$, $D = 8.0$) as the base, respectively. The values of N are chosen to be 100, 130, 150, 180, 200, and 250. The solid lines are drawn to scaling fit. The inset in (a) shows dependency of the exponent of induction α_{in} with κ, while the inset in (b) belongs to dependency of the exponent of segregation α_{se} with κ. And κ is set to 3.125, 3.904, 5.047, 6.840, and 9.921. Each value of κ is obtained from the scaling fit of 6 independent (N, D) sets.

Nevertheless, the landscape $U(x, y)$ obtained in the present work still helps us to get more insight about the system dynamics. As discussed above, $U(x, y) = \kappa u(x, y)$, where $u(x, y)$ is not dependent on N and D such that U would be the same, given that κ is a constant. In this case, the whole dynamics would be dependent on the value of $\mathcal{D}$ only. It is thus instructive to investigate the behavior of $\bar{t}_{in}$ or $\bar{t}_{se}$ for different fixed values of κ, which would reflect some information about the diffusion coefficient $\mathcal{D}$. In Fig. 8, the dependencies of (a) $\bar{t}_{in}$ and (b) $\bar{t}_{se}$ on the chain length N are depicted, obtained from direct MD simulations. Rather interestingly, both $\bar{t}_{in}$ and $\bar{t}_{se}$ show good power-law scaling with N, i.e., $\bar{t}_{in} \sim N^{\alpha_{in}}$ and $\bar{t}_{se} \sim N^{\alpha_{se}}$, for fixed κ. The insets in (a) and (b) show the dependencies of the exponents α_{in} and α_{se} on κ (with error bars) for the induction and segregation times, respectively. It seems that α_{in} is nearly a constant around 2.75 and α_{se} also reaches a constant about 2.35 for large κ.

According to the discussions made above, both $\bar{t}_{in}$ and $\bar{t}_{se}$ should be proportional to $\mathcal{D}^{-1}$ if the potential landscape is fixed (κ = const). One would then expect that the scaling of $\bar{t}_{in}$ and $\bar{t}_{se}$ with N also suggest the scaling of $\mathcal{D}$ with N, and the scaling exponent should be the same for $\bar{t}_{in}$ and $\bar{t}_{se}$ if the free energy landscape $U(x, y)$ is accurate and the Fokker-Planck Eq. (7) works well. However, our simulation results show discrepancies between α_{in} and α_{se}, which suggests that the free energy landscape $U(x, y)$ is still an approximation. Another reason might be that the motion of the effective particle on the landscape cannot be described by a constant $\mathcal{D}$, i.e., $\mathcal{D}$ might be a function of $\mathbf{r} = (x, y)$. Nevertheless, the simulation results demonstrate that $\mathcal{D} \sim N^{-\alpha}$, while the exponent α is different for induction and segregation.

F. Scaling of $\bar{t}_{in}$ and $\bar{t}_{se}$

The above analysis indicates that it is not straightforward to obtain a scaling form for $\bar{t}_{in}$ (or $\bar{t}_{se}$) as a function of N. For fixed κ, it suggests by direct MD simulations that both $\bar{t}_{in}$ and $\bar{t}_{se}$ show power-law dependencies on N, as demonstrated in the last paragraph, but with different scaling exponents dependent on κ. Such dependencies should give some information about the diffusion coefficient $\mathcal{D}$ used in the Fokker-Planck equation or corresponding Brownian simulations, i.e., $\mathcal{D} \sim N^{-\alpha(\kappa)}$. If we fix $\mathcal{D} = 1$ and using Brownian simulations based on the 3D landscape obtained in our work, we find that both $\bar{t}_{in}$ and $\bar{t}_{se}$ show very good power-law decreasing dependencies on κ, in contrast to previous studies where one end of the polymer chains was fixed. Note that such a power-law dependence cannot be checked directly by MD simulations since it is hard to figure out a way to fix $\mathcal{D}$ in MD.

Combining these information together, it seems that one can suggest a scaling ansatz for the average induction time $\bar{t}_{in}$ or the segregation time $\bar{t}_{se}$ as follows:

$$\bar{t}_{in/se} \sim N^{\alpha(\kappa)} \kappa^{c}, \tag{9}$$

wherein the scaling exponent $\alpha(\kappa)$ is generally a function of κ and different for induction and segregation, $c < 0$ is a constant independent of κ. For fixed κ, both $\bar{t}_{in}$ and $\bar{t}_{se}$ show power-law scaling with N. While for fixed N, the dependence on κ is complicated, since the exponent α also depends on κ. On the whole, one cannot obtain a simple scaling with N, in contrast to previous studies reported in Refs. 18 and 23.

V. DISCUSSION

Before Sec. VI, some discussions on the limits of theoretical approximation made in the current work are salutary. Note that the analytical expression for the free energy landscape $U(x, y) \sim N/D^{5/3} u(x, y)$ summarized in Eqs. (4)–(6) is central to this study and its derivation rests on the validity of the de Gennes blob model and the accuracy of scaling exponent v in such a highly confined environment. Indeed, such a blob scenario may not strictly work as increasing the level of confinement or increasing $\kappa (\kappa = N/D^{1/v}, v \simeq 3/5)$. Along with it is the deviation of v because of the increasing crowding. Kim *et al.* showed that for flexible FENE-chain model polymers, the strict de Gennes scaling relation (for the blob model) with respect to N and D would emerge for sufficiently large channels D and for sufficiently long polymers such that both the number of monomers per blob and the number of blobs are large enough.[31] In consideration of computational efficiency, many of the simulations in the present study use channel widths (and polymer lengths as well) that are not in

the regime where the predicted scaling exponent is likely to be accurate. Besides, in a very recent study by Polson *et al.*, it was shown that the scaling exponent v in such a highly confined case is probably something more like 0.53 (close to Gaussian chain scaling, $v = 0.5$), which was calculated directly using Monte Carlo simulations.[32] Consequently, $v = 3/5$ of the calculated free energy function $U(x, y)$ may not be particularly accurate. In addition, the predicted form of $U(x, y)$ could also be inaccurate.

Actually these latent effects has been shown in Figs. 7(a) and 7(b), where the density distribution is not strictly concentrated along $x + y = 0.065$ which is the energy minimum based on the function of $U(x, y)$. In Figs. 6(a) and 6(b), BD results and direct MD simulation results also present quantitative differences. For a probably compromise solution, a more generalized free energy scaling may look like $U(x, y) \sim N^a D^b u(x, y)$, where a and b are adjustable scaling exponents based on the system confinement, while still maintaining the concise form of $u(x, y)$. Nevertheless, in spite of the theoretical approximations made, we believe that the underlying physical picture depicted the global dynamic behaviors and such a new induction mechanism should be qualitatively unaffected.

VI. CONCLUSION

In summary, we have studied the separation process of two identical polymer chains in a cylindrical confinement under the framework of a three dimensional (3D) free energy landscape $U(x, y)$ obtained by renormalized blob theory, which is a function of two free parameters x and y, the number fraction of overhanging monomers at the two ends of one chain over another. The landscape gives a clear picture how the induction and segregation would take place in the whole process. An important feature of the free energy function $U(x, y)$ is that it can be written as the product of a parameter $\kappa = ND^{-5/3}$ and a function $u(x, y)$ that is not system-dependent. Therefore, the free energy landscape would be the same if one introduces the so-called *blob constraint*, i.e., κ = const. The free energy picture also allows one to study the system dynamics by using an over-damped Langevin equation corresponding to the Fokker-Planck equation. And the validity of the free energy landscape was further confirmed by both direct molecular dynamic simulations and effective Brownian dynamic simulations.

Besides, such a free energy landscape suggests that the induction process is distinct from either the barrier-crossing mechanism suggested by Minina and Arnold in Refs. 24 and 23 or the diffusion mechanism suggested in an earlier study.[18] In Sec. IV F, we have given a ansatz for both the average induction and segregation times $\bar{t}_{in/se} \sim N^{\alpha(\kappa)}\kappa^c$ ($c < 0$) to conclude our findings, which describes the scaling with respect to the polymer length N as well as the "*blob constraint*" $\kappa = N/D^{-5/3}$, which plays an important role in this theoretical picture. We believe that our work can open more perspectives on the study of polymers confined in cylindrical geometry and may shed some new lights on understanding such an important process in real biological systems.

ACKNOWLEDGMENTS

This work is supported by the National Basic Research Program of China (Grant No. 2013CB834606), by the National Science Foundation of China (Grant Nos. 21125313, 21521001, 21473165, and 21403204), and by the Fundamental Research Funds for the Central Universities (Grant Nos. WK2060030018, 2030020028, and 2340000074).

APPENDIX: The derivation of free energy landscape

According to the Flory theory, a polymer with N monomers confined in a cylinder with diameter D can be equivalent to a sequence of blobs arranged closely,[2] wherein one blob consists of $g \sim D^{1/v}$ ($v \simeq 3/5$ in three dimensions) monomers each with free energy f_b, which is a non-universal constant depending on the type of polymer. The chain thus has $n_b = N/g$ blobs, and the total free energy of the chain is given by

$$U = n_b f_b \sim ND^{-5/3} f_b. \tag{A1}$$

The extended length of the chain is given by

$$L = n_b D \sim ND^{-2/3}. \tag{A2}$$

We consider two identical polymer chains, in which blue polymer labeled 1 and red polymer labeled 2, confined in a cylinder with diameter D with an initial (I) state shown in Fig. 1(a). By using the renormalized Flory theory,[29] the overlapped parts of two polymers can be treated as two single polymers trapped in effective sub-cylinders of diameters $D_1 = D\sqrt{\alpha}$ and $D_2 = D\sqrt{1-\alpha}$,[23,24,30] respectively, where α denotes a partition coefficient. For this fully overlapped initial state, $\alpha = 1/2$ and $D_1 = D_2 = D/\sqrt{2}$, and each polymer contains $n_b \sim N\left(D/\sqrt{2}\right)^{-5/3}$ blobs. The free energy of this initial state is given by

$$U_I = 2^{11/6} ND^{-5/3} f_b \tag{A3}$$

In this system, the monomers overhang at two sides are N_x and N_y. To avoid ambiguity, we define that if any one end of polymer 2 is covered by the corresponding end of polymer 1, $N_x(N_y) > 0$, else $N_x(N_y) < 0$. As to the trapped (T) state shown in Fig. 1(b), for the case both $N_x > 0$ and $N_y > 0$ such that polymer 2 is totally trapped into polymer 1. In the middle overlapped region, the number of monomers is $N - N_x - N_y$ for polymer 1 and N for polymer 2, trapped in effective sub-cylinders with diameters $D_1 = D\sqrt{\alpha_T}$ and $D_2 = D\sqrt{1-\alpha_T}$, respectively, where α_T denotes the partition coefficient for this T-state. Note that the extended lengths of both polymers are the same in the overlapped region, i.e.,

$$\left(N - N_x - N_y\right)(D_1)^{-2/3} = N(D_2)^{-2/3}, \tag{A4}$$

which gives that

$$\alpha_T = \frac{\left(N - N_x - N_y\right)^3}{N^3 + \left(N - N_x - N_y\right)^3} = \frac{(1-x-y)^3}{1 + (1-x-y)^3}, \tag{A5}$$

where $x = N_x/N$ and $y = N_y/N$. The free energy of polymer 1 in the T-state is then given by

$$U_{T,1} = N_x D^{-5/3} + \left(N - N_x - N_y\right)(D_1)^{-5/3} + N_y D^{-5/3}, \quad \text{(A6)}$$

where the three terms correspond to the left overhanged part, the middle overlapped part, and the right overhanged part, respectively. The free energy of polymer 2 in this T-state is

$$U_{T,2} = N(D_2)^{-5/3}. \quad \text{(A7)}$$

Substituting D_1 and D_2 with the obtained α_T, we can obtain the free energy of the T-state as a function of x and y (for $x > 0$ and $y > 0$)

$$U_T(x,y) = ND^{-5/3}\left[(1-x-y)\alpha_T^{-5/6} + (1-\alpha_T)^{-5/6} + x + y\right], \quad \text{(A8)}$$

$$= ND^{-5/3}\left\{\left[1 + (1-x-y)^3\right]^{5/6}\left[1 + (1-x-y)^{-3/2}\right] + x + y\right\} \text{ for } (x > 0, y > 0). \quad \text{(A9)}$$

If $x < 0$ and $y < 0$, the polymer 1 is trapped into polymer 2. One can easily get $U_T(x,y) = U_T(-x,-y)$ due to the symmetry.

Note that if $N_x > 0$ and $N_y < 0$, as shown in Fig. 1(c), the two polymers are in a released (R) state and the segregation process may start. Similar to the above procedures, we can obtain the free energy of the two polymers as

$$U_{R,1} = N_x D^{-5/3} + (N - N_x)\left(D\sqrt{\alpha_R}\right)^{-5/3} \quad \text{(A10)}$$

and

$$U_{R,2} = \left(N - \left|N_y\right|\right)\left(D\sqrt{1-\alpha_R}\right)^{-5/3} + \left|N_y\right|D^{-5/3}. \quad \text{(A11)}$$

The partition coefficient α_R can be obtained via equal of the extended length in the overlapped region

$$(N - N_x)(\alpha_R)^{-2/3} = \left(N - \left|N_y\right|\right)(1-\alpha_R)^{-2/3}, \quad \text{(A12)}$$

which gives

$$\alpha_R = \frac{(1-x)^3}{(1-x)^3 + (1+y)^3} \quad \text{(A13)}$$

for $x > 0$ and $y < 0$. The total free energy of the R-state is then

$$U_R(x,y) = ND^{-5/3}\left[(1-x)\alpha_R^{-5/6} + (1+y)(1-\alpha_R)^{-5/6} + x - y\right], \quad \text{(A14)}$$

$$= ND^{-5/3}\left\{\left[(1-x)^3 + (1+y)^3\right]^{5/6}\left[(1-x)^{-3/2} + (1+y)^{-3/2}\right] + x - y\right\}, \text{ for } (x > 0, y < 0). \quad \text{(A15)}$$

While for $x < 0$ and $y > 0$, one can also obtain that $U_R(x,y) = U_R(-x,-y)$ due to the symmetry.

Finally, we can write the free energy of the trapped state as

$$U_T(x,y) = ND^{-5/3}\left\{\left[1 + (1 - |x| - |y|)^3\right]^{5/6} \times \left[1 + (1 - |x| - |y|)^{-3/2}\right] + |x| + |y|\right\} \text{ for } xy \geq 0. \quad \text{(A16)}$$

Similarly, the free energy of the release state is given by

$$U_R(x,y) = ND^{-5/3}\left\{\left[(1-|x|)^3 + (1-|y|)^3\right]^{5/6} \times \left[(1-|x|)^{-3/2} + (1-|y|)^{-3/2}\right] + |x| + |y|\right\}, \text{ for } xy \leq 0. \quad \text{(A17)}$$

[1] M. Rubinstein and R. H. Colby, *Polymer Physics* (Oxford University Press, New York, 2003), Vol. 23.
[2] P.-G. De Gennes and P.-G. Gennes, *Scaling Concepts in Polymer Physics* (Cornell University Press, 1979).
[3] K. H. Rasmussen, R. Marie, J. M. Lange, W. E. Svendsen, A. Kristensen, and K. U. Mir, Lab Chip **11**, 1431 (2011).
[4] J. Pelletier, K. Halvorsen, B.-Y. Ha, R. Paparcone, S. J. Sandler, C. L. Woldringh, W. P. Wong, and S. Jun, Proc. Natl. Acad. Sci. U. S. A. **109**, E2649 (2012).
[5] W. Reisner, J. N. Pedersen, and R. H. Austin, Rep. Prog. Phys. **75**, 106601 (2012).
[6] L. Dai and P. S. Doyle, Macromolecules **46**, 6336 (2013).
[7] Y. Hu, R. Zandi, A. Anavitarte, C. M. Knobler, and W. M. Gelbart, Biophys. J. **94**, 1428 (2008).
[8] M. Fritsche, S. Li, D. W. Heermann, and P. A. Wiggins, Nucl. Acids Res. **40**, 972 (2011).
[9] S. Jun and A. Wright, Nat. Rev. Microbiol. **8**, 600 (2010).
[10] A. Muralidhar, D. R. Tree, Y. Wang, and K. D. Dorfman, J. Chem. Phys. **140**, 084905 (2014).
[11] D. Račko and P. Cifra, J. Chem. Phys. **138**, 184904 (2013).
[12] Z. Benkova and P. Cifra, Macromolecules **45**, 2597 (2012).
[13] Y. Chen, W. Yu, J. Wang, and K. Luo, J. Chem. Phys. **143**, 134904 (2015).
[14] O. Espeli, R. Mercier, and F. Boccard, Mol. Microbiol. **68**, 1418 (2008).
[15] J. Kim, C. Jeon, H. Jeong, Y. Jung, and B.-Y. Ha, Soft Matter **11**, 1877 (2015).
[16] C. Jeon, Y. Jung, and B.-Y. Ha, Sci. Rep. **7**, 11896 (2017).
[17] J. Sheng and K. Luo, Phys. Rev. E **86**, 031803 (2012).
[18] A. Arnold and S. Jun, Phys. Rev. E **76**, 031901 (2007).
[19] J. M. Polson, A. F. Tremblett, and Z. R. McLure, Macromolecules **50**, 9515 (2017).
[20] D. Bates and N. Kleckner, Cell **121**, 899 (2005).
[21] C. Lesterlin, E. Gigant, F. Boccard, and O. Espeli, EMBO J. **31**, 3468 (2012).
[22] M. C. Joshi, D. Magnan, T. P. Montminy, M. Lies, N. Stepankiw, and D. Bates, PLoS Genet. **9**, e1003673 (2013).
[23] E. Minina and A. Arnold, Soft Matter **10**, 5836 (2014).
[24] E. Minina and A. Arnold, Macromolecules **48**, 4998 (2015).
[25] L. Postow, C. D. Hardy, J. Arsuaga, and N. R. Cozzarelli, Genes Dev. **18**, 1766 (2004).
[26] J. D. Weeks, D. Chandler, and H. C. Andersen, J. Chem. Phys. **54**, 5237 (1971).
[27] K. Kremer and G. S. Grest, J. Chem. Phys. **92**, 5057 (1990).
[28] H.-J. Limbach, A. Arnold, B. A. Mann, and C. Holm, Comput. Phys. Commun. **174**, 704 (2006).
[29] S. Jun, D. Thirumalai, and B.-Y. Ha, Phys. Rev. Lett. **101**, 138101 (2008).
[30] Y. Jung, C. Jeon, J. Kim, H. Jeong, S. Jun, and B.-Y. Ha, Soft Matter **8**, 2095 (2012).
[31] J. Kim, C. Jeon, H. Jeong, Y. Jung, and B.-Y. Ha, Soft Matter **9**, 6142 (2013).
[32] J. M. Polson and D. R.-M. Kerry, Soft Matter **14**, 6360 (2018).